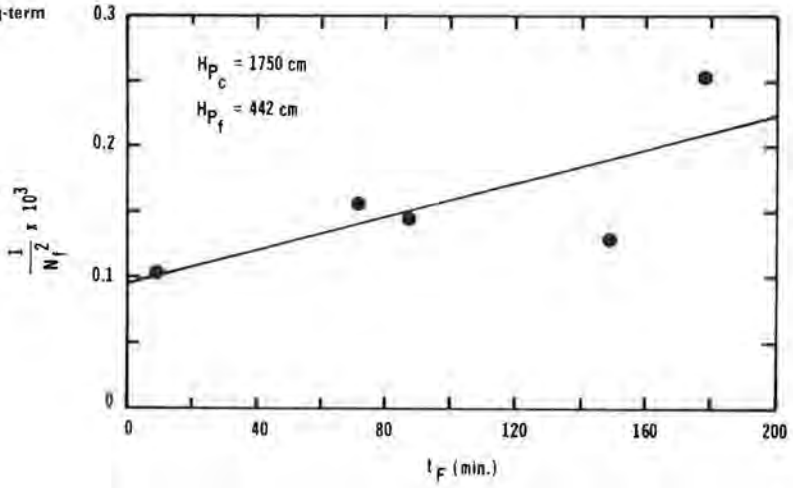

Figure 12. Time to failure versus $1/N_f^2$ for long-term modeling-of-model test.

REFERENCES

1. R. Fragaszy and J.A. Cheney. Drum Centrifuge Studies of Overconsolidated Slopes. Journal of Geotechnical Engineering Division of ASCE, Vol. 107, No. GT7, 1981, pp. 843-858.
2. R. Fragaszy. Drum Centrifuge Studies of Overconsolidated Clay Slopes. Univ. of California, Davis, Ph.D. dissertation, 1979.
3. N. Krebs-Ovesen. Centrifuge Testing Applied to Bearing Capacity Problems of Footings on Sand. Geotechnique, Vol. 25, 1975, pp. 344-401.
4. N. Krebs-Oveson. The Scaling Law Relationships. Proc., Seventh European Conference on Soil Mechanics and Foundation Engineering, Brighton, England, 1979, Vol. 4, pp. 319-323.
5. N. Krebs-Oveson. Centrifuge Tests to Determine the Uplift Capacity of Anchor Slabs in Sand. Proc., 10th International Conference on Soil Mechanics and Foundation Engineering, Stockholm, Sweden, 1981.
6. A.N. Schofield and C.P. Wroth. Critical State Soil Mechanics. McGraw-Hill, London, 1968.
7. A.W. Skempton. Slope Stability of Cuttings in Brown London Clay. Proc., Ninth International Conference on Soil Mechanics and Foundation Engineering, Tokyo, Vol. 3, Special Lectures, 1977, pp. 261-270.
8. J.D. Nelson and E.G. Thompson. A Theory of Creep Failure in Overconsolidated Clay. Journal of the Geotechnical Engineering Division of ASCE, Vol. 103, No. GT11, 1977, pp. 1281-1294.

Publication of this paper sponsored by Committee on Mechanics of Earth Masses and Layered Systems.

Centrifugal Testing of Soil Slope Models

MYOUNG MO KIM AND HON-YIM KO

The principles of testing static geomechanical models are explained, and the need to simulate the gravity-induced body forces is emphasized. The only convenient method of inducing increased gravity on models of soil structures is to spin the model in a centrifuge. Experiments were conducted in a 10-*g*-ton geotechnical centrifuge to model the stability of slopes of partly saturated granular soils. A series of modeling-of-models tests was conducted in which several models of different scales were tested at different gravity scales. The internal consistency of the centrifugal modeling technique is demonstrated by results of these tests, which show that the same critical height of the prototype slope is obtained irrespective of model scale. A quantitative comparison is made of the model test data and analytical results from limit analysis, finite-element analysis, and limiting-equilibrium analysis. It is demonstrated that the critical slope heights obtained from the centrifuge tests are bracketed within the upper bounds established by limit analysis and the lower bounds obtained from finite-element calculations. In addition, the locations of the failure surface obtained by testing and analysis correspond closely in all cases.

Testing of scaled earth models under an increased gravitational body force field is a relatively new idea in soil mechanics. This centrifugal-modeling technique is the only method that can completely satisfy the requirements of the principles of similitude in the geotechnical model in which body forces of a structure are significant. Nevertheless, many workers are still unconvinced of the validity of the method, primarily due to the lack of prototype data against which model behavior can be compared. Even when such data are available, comparisons usually point out the necessity to better define the geology of the prototype situation as well as the material properties.

In order to demonstrate that the scaled centrifugal model can project to prototype behavior, it is possible to carry out a modeling of models, in which a series of models is constructed at different scales, all representing the same prototype (which could be an imaginary situation), and tested at different gravity ratios, each calculated to bring the respective model to full similitude with the prototype. Only when it has been demonstrated that

Figure 1. Failure envelope and stress-strain curves of prototype and model materials.

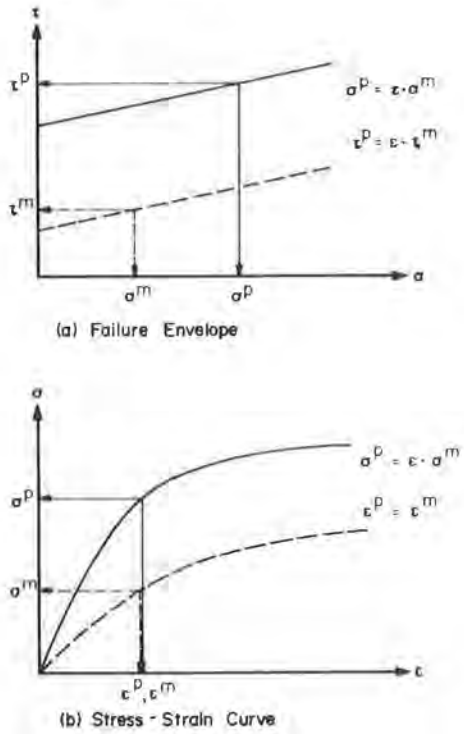

all models produce the same prototype projections can it be considered that the scaling relations obtained from the principles of similitude are valid and are therefore invariant with respect to the model scale. A homogeneous slope of granular soil is chosen to be the test model in this investigation. Three series of slope models of different sizes that had similar geometry were built and tested in a centrifuge.

After the concept of the modeling of models has been confirmed by using the slope model, the next step is to compare the self-consistent results of the centrifuge tests with the solutions obtained by analytical methods to verify the validity of the model test results on a quantitative basis. To this end, the stability of the centrifuged slope is analyzed by the upper-bound method in limit analysis. Solutions obtained by the finite-element method and the simplified Bishop's method of limiting equilibrium analysis are compared with the test results in terms of the critical height and/or the location of the failure surface of the slope.

BACKGROUND

In general, physical models can be grouped into two categories depending on whether they satisfy the principles of similitude or not (1). In order to predict the behavior of the prototype on a quantitative basis by using model test data, however, the principles of similitude should always be satisfied in the model system.

If the principles of similitude are satisfied in the model, one can pass from a certain quantity y' derived from the model to a homologous quantity y in the prototype by means of a scale factor that is fixed by similitude. In problems of statics there are two independent quantities, length and specific force (force per unit area); therefore, two independent scale factors for the respective quantities involved may be defined as follows:

$$\lambda = L/L' \qquad \xi = \sigma/\sigma' \tag{1}$$

where

λ, ξ = scale factors for length and specific force, respectively;
L, σ = length and specific force in prototype; and
L', σ' = length and specific force in model.

It may be noted that the length scale λ must also be valid for displacement and that the scale factor of specific force ξ must be valid for all quantities having the dimensions of specific force, for example, modulus of elasticity E and shear stress τ.

Since the scale factor of length λ is always greater than unity for practical geotechnical models, only two types of models, when they are classified with respect to the magnitude of the scale factors, are possible in the modeling of such problems. They are (a) models in which the scale factor of the specific force ξ is greater (or smaller) than 1 and (b) models in which the scale factor of the specific force ξ is equal to 1.

The first type of modeling requires that the failure envelopes of the model and prototype materials must be geometrically similar with respect to the origin of the axes in the Mohr diagram, as shown in Figure 1a (1), according to the following relations:

$$\sigma = \xi\sigma' \qquad \tau = \xi\tau' \tag{2}$$

At the same time, the stress-strain curves of the prototype and model materials must also correspond as shown in Figure 1b, according to the following relations:

$$\sigma = \xi\sigma' \qquad \varepsilon = \varepsilon' \tag{3}$$

In earth structures, however, it is extremely difficult, if not impossible, to satisfy these two critical conditions imposed on the model material.

In the second case, the material of the prototype can be used for the model provided that body forces can be ignored when compared with boundary forces. However, body forces are almost invariably significant in soil-mechanics prototype problems, and the investigator is then faced with the requirements of the similarity of body forces. The scale factor of body forces η may be expressed as follows:

$$\eta = \gamma/\gamma' = (\sigma \cdot L^{-1})/[\sigma' \cdot (L')^{-1}] = \xi \cdot \lambda^{-1} \tag{4}$$

where γ and γ' are the unit weights of prototype and model materials, respectively. Substituting $\xi = 1$ into Equation 4, we obtain the following:

$$\eta = \gamma/\gamma' = \lambda^{-1} \tag{5}$$

that is to say,

$$\gamma' = \gamma \cdot \lambda \tag{6}$$

Equation 6 implies that the unit weight of model material should be as many times greater than the length scale λ than the unit weight of prototype material. Furthermore, this model material should have the same mechanical properties with respect to both strength and stress-strain behavior as the prototype material, since the scale factor of specific force ξ is now equal to unity. Again, it is impossible to find such a model material that satis-

fies these requirements without introducing a special technique by which the unit weight of model material can be increased as many times as required.

By using a centrifugal modeling scheme, in which the material of the prototype is used for the model, one can satisfy these requirements. By the definition of the unit weight, $\gamma = \rho \cdot \underline{g}$, where ρ is mass per unit volume and $\underline{g}$ is acceleration of the gravity force. Substituting this into Equation 6, we get the following:

$$\gamma' = \rho \cdot g \cdot \lambda = \rho \cdot a \tag{7}$$

where $a = \lambda \cdot \underline{g}$. Therefore, if the magnitude of the acceleration of the gravity force $\underline{g}$ can be magnified as many times as the scale factor of length λ in the model system, the principles of similitude will be satisfied. The magnification of the acceleration field can be achieved easily in a centrifuge, where a centrifugal acceleration of the force of inertia is generated.

EQUIPMENT

The centrifuge used in this investigation is a modified version of the Genisco Model 1230-5G accelerator at the University of Colorado. The centrifuge system is shown in Figure 2. The effective radius of the centrifuge is 53.5 in measured to the base of the swinging basket, and the weight capacity is 20 000 $\underline{g}$-lb. The essential features of this centrifugal system are described below.

Of the two swinging baskets hinged to the ends of the rotating arm, one (3, Figure 2) was used to mount the test package consisting of a specimen container (4) and a mirror system (5). The other (6) was used as a counterweight mount to balance the centrifuge dynamically as well as statically. The maximum dimensions of the allowable test package on the basket are 18x18x12 in.

The closed-circuit television camera is mounted close to the centrifuge axis and is focused on the test package through the mirror system so that the behavior of a model structure in the specimen container during the experiment can be observed. The experiment can be recorded by a video tape recorder outside the centrifuge. In addition, two hydraulic rotary joints are available in this system for hydraulic power transmission into the centrifuge for driving jacks, for instance, but they were not used in these experiments.

TEST PROGRAMS AND PROCEDURES

Three series of plane strain slope models were constructed and tested in the centrifuge. The slopes in each series had a similar geometry with the same slope angle (60°) but with different heights (8, 4, or 2.67 in), as shown in Figure 3. Two kinds of granular soils, identified as A and B, were used in the construction of slopes. They were artificially batched in the laboratory according to the gradation curves, which were chosen arbitrarily. For both soils, 5 percent of moisture was introduced to create the apparent cohesion as a result of the negative pore-pressure development.

The specimen container has the inside dimensions 16x11.5x6 in. The front wall of the container was made of lucite plate 1 in thick so that a model slope inside the container could be seen through the wall, while the other three walls and the base were made of aluminum plate 0.5 in thick. The lucite wall has a 1-in^2 grid scribed on its inside surface, which is used as a datum for marking the shape of the failure surface after a slope failure. Wood formworks of three sizes were used to define the geometries of the model slopes.

The model slopes were constructed in the following manner:

1. The container was laid horizontally with the front lucite wall removed.
2. A wood formwork was clamped down in the proper position according to the specified geometry of the slope to be built.
3. Dry soil and 5 percent of water by weight were mixed, and the mixed soil was compacted in layers in the specimen container.
4. The lucite wall was attached to the container, which was then erected to its testing position.

After being located in the centrifuge, slope test models were accelerated by increasing the rotational velocity of the centrifuge until failure. Each individual test was monitored by the TV video system through the failure stage.

MODEL TEST RESULTS

If the scaling relations derived from the principles of similitude are to be observed in centrifugal model testing, all three series of the model slopes of similar geometry, built of the same soil at the same density, should predict identical prototype behavior in terms of the critical height of the slope, which can be obtained by the following expression:

$$H_c^p = H_m \times (a/g) \tag{8}$$

where H_c^p is the predicted critical height of the prototype slope, H_m is the height of the model slope at failure, when the centrifugal acceleration reached the value a, and $\underline{g}$ is the acceleration of the gravity force. However, the densities of the soils in the test models could not be controlled exactly for all the model slopes tested in this study; therefore, the critical heights calculated would not all be identical but are a function of soil densities, as the strength of soils is. With this in mind, the results of the three series of model tests listed in Tables 1 and 2 and plotted in Figures 4 and 5 can now be examined.

In Figures 4 and 5, best least-squares-fit lines are drawn through the data points of each series of models. It is noticed from the fitted lines that there is a trend showing that the H_c^p values increase as the density of the slope soil increases, as expected.

Comparisons are made among the results of the three series at the middle of the density range, 108.5 pcf and 101.0 pcf for soils A and B, respectively. At that density, the average value of the predicted critical height is calculated from the fitted lines, and deviations from this average for each of the three model scales are calculated. Thus, it is shown in Figures 4 and 5 that the 4-in model predicted a critical height of the prototype to be 8.3 percent higher and the 8-in model predicted a height 11.5 percent lower than the average value for soil A, while for soil B the predicted critical height by the 2.67-in model is higher by 6.2 percent and that by the 8-in model is lower by 10.2 percent than the average value of the H_c^p at the soil density of comparison. Such scatter is considered to be negligible in engineering applications, and it is concluded that all three series of the model slopes predict identical prototype behavior in terms of its

Figure 2. Centrifugal system used in experiments: 1, slip-ring assembly; 2, closed-circuit TV camera; 3, test package basket; 4, specimen container; 5, mirror system; 6, counterweight basket.

Figure 3. Configuration of model slope.

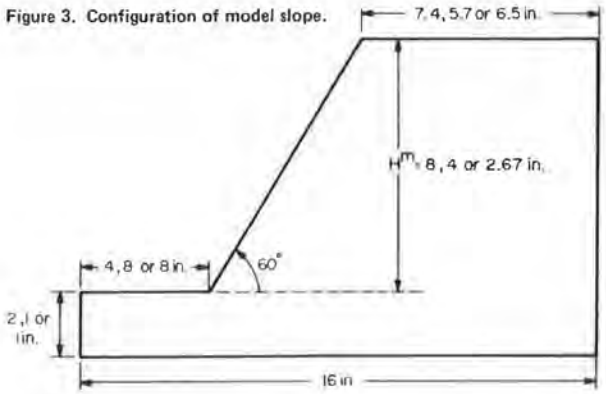

critical height. Thus, the concept of modeling of models is confirmed.

In Figure 6, the failure surface observed from the centrifugal slope model tests is shown in the form of a band bracketing the locations observed in all the tests. This will be compared later with the failure surfaces obtained by analytical methods.

SLOPE STABILITY ANALYSIS BY ANALYTICAL METHODS

To examine quantitatively the validity of the results of the centrifugal slope model tests, the stability problem of the centrifuged slope is solved by the analytical methods such as the upper-bound method in limit analysis, the finite-element method, and the simplified method in limiting-equilibrium analysis, and the results of these analyses are compared with the model test results.

Limit Analysis

In solving the stability problem by the upper-bound method in limit analysis, a rotational failure mechanism is assumed in this study, as shown in Figure 7, in which the failure surface passes through the toe of the slope. In Figure 7, the triangular region ABC rotates as a rigid body about the center of rotation 0; the materials below the logarithmic surface BC remain at rest.

To obtain an upper bound for the critical value of the height of the slope in Figure 7, the external rate of work done by the soil mass ABC is equated to the internal energy dissipation along the surface BC, which gives the following expression (2):

$$H = (c/\gamma)\, f(\theta_b, \theta_t) \tag{9}$$

where the function $f(\theta_b, \theta_t)$ is defined as follows:

$$f(\theta_b, \theta_t) = \left\{ \exp[2(\theta_b - \theta_t)\tan\phi]/2\tan\phi(f_1 - f_2 - f_3) \right\} \left\{ \sin\theta_b \exp[(\theta_b - \theta_t)\tan\phi] - \sin\theta_t \right\} \tag{10}$$

in which θ_b and θ_t are as defined in Figure

Table 1. Test results for soil A.

Specimen Number	Unit Weight (pcf)	a/g at Failure	Predicted H_c^p (in)	Water Content[a] (%)
8-in Model				
A-8-1	109.21	32.3	258.4	4.72
A-8-2	109.21	29.1	232.8	4.42
A-8-3	108.55	25.2	201.6	4.05
A-8-4	109.21	24.4	195.2	4.85
A-8-5	109.21	30.3	242.4	3.94
A-8-6	107.89	21.2	169.6	3.66
A-8-7	111.84	41.4	331.2	4.29
A-8-8	110.26	30.3	242.4	4.92
A-8-9	109.67	27.5	220.0	5.41
A-8-10	107.81	27.5	220.0	4.68
4-in Model				
A-4-1	107.62	54.5	218.0	4.69
A-4-2	107.62	67.5	270.0	4.58
A-4-3	105.96	43.3	173.2	4.43
A-4-4	109.27	65.7	262.8	5.07
A-4-5	107.28	52.2	208.8	5.47
2.67-in Model				
A-8/3-1	108.94	105.8	282.5	4.55
A-8/3-2	106.50	70.8	189.0	5.26
A-8/3-3	107.32	74.0	197.6	4.28
A-8/3-4	108.94	86.4	230.7	4.12
A-8/3-5	106.50	61.5	164.2	4.63

[a]Water content was measured immediately after testing.

Table 2. Test results for soil B.

Specimen Number	Unit Weight (pcf)	a/g at Failure	Predicted H_c^p (in)	Water Content[a] (%)
8-in Model				
B-8-1	101.32	18.0	144.0	4.73
B-8-2	101.32	17.3	138.4	4.74
B-8-3	101.84	17.6	140.8	4.80
B-8-4	100.66	16.4	131.2	4.43
B-8-5	101.32	20.9	167.2	4.57
B-8-6	101.32	23.4	187.2	4.46
4-in Model				
B-4-1	98.68	32.1	128.4	5.05
B-4-2	100.00	39.4	157.6	4.62
B-4-3	100.66	37.0	148.0	4.96
B-4-4	100.66	43.8	175.2	4.41
B-4-5	101.32	45.3	181.2	4.93
2.67-in Model				
B-8/3-1	101.63	64.5	172.2	4.60
B-8/3-2	100.81	57.9	154.6	5.19
B-8/3-3	99.19	52.8	141.0	4.72
B-8/3-4	100.00	70.8	189.0	4.51
B-8/3-5	100.81	72.7	194.1	4.48

[a]Water content was measured immediately after testing.

Figure 4. Results of centrifugal slope model tests, soil A.

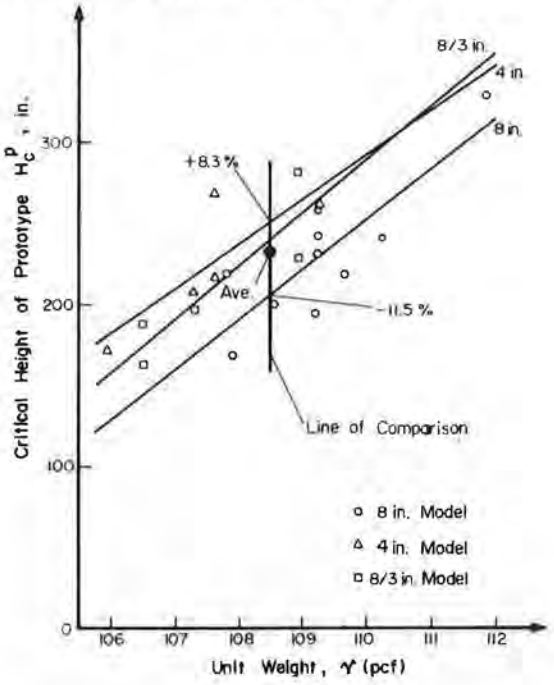

Figure 5. Results of centrifugal slope model tests, soil B.

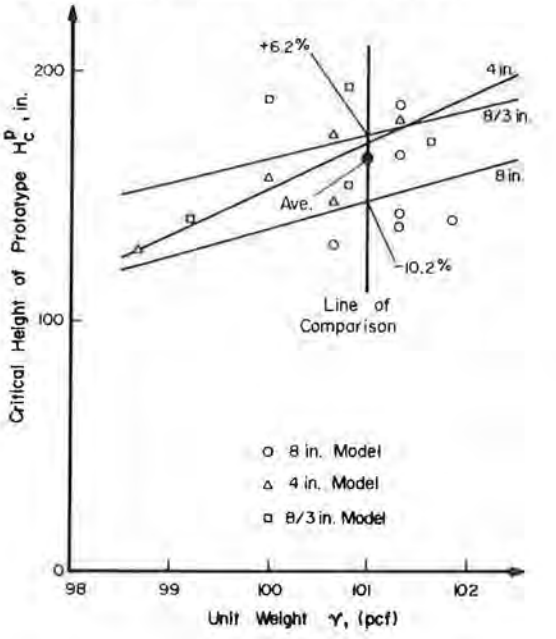

7, ϕ is the friction angle, and the following expressions hold:

$$f_1(\theta_b,\theta_t) = [1/3(1+9\tan^2\phi)]\,(3\tan\phi\cos\theta_b + \sin\theta_b)\exp[3(\theta_b - \theta_t)\tan\phi - (3\tan\phi\cos\theta_t + \sin\theta_t)] \quad (11)$$

$$f_2(\theta_b,\theta_t) = (1/6)(L/r_t)[2\cos\theta_t - (L/r_t)]\sin\theta_t \quad (12)$$

$$f_3(\theta_b,\theta_t) = (1/6)\exp[(\theta_b-\theta_t)\tan\phi]\,[\sin(\theta_b-\theta_t)(L/r_t)\sin\theta_b]\cos\theta_t - (L/r_t) + \cos\theta_b\,[\exp(\theta_b-\theta_t)\tan\phi] \quad (13)$$

L and r_t are also defined in Figure 7.

A least upper bound for the critical height of the slope may be obtained by finding a minimum value

Figure 6. Failure surface of centrifugal model slope.

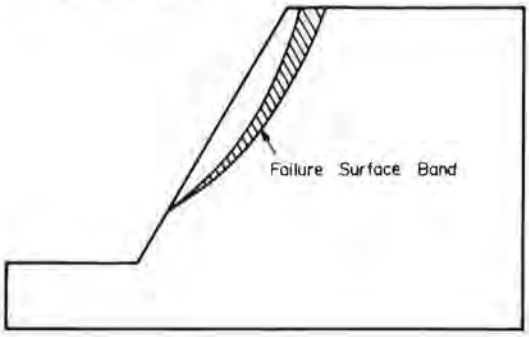

Figure 7. Failure mechanism for stability of embankment with failure plane passing through toe.

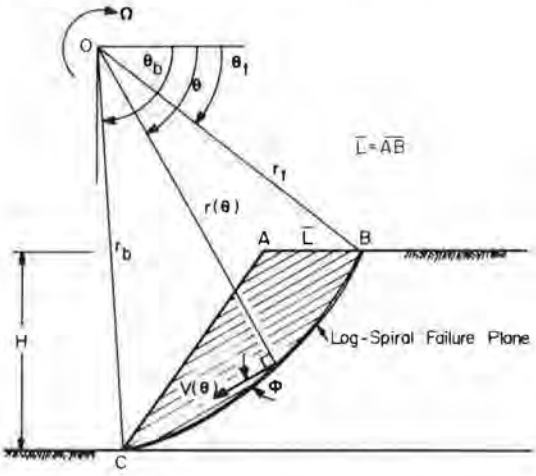

of the function $f(\theta_b,\theta_t)$, i.e.,

$$H_c = (c/\gamma)\min[f(\theta_b,\theta_t)] = (c/\gamma)N_s \quad (14)$$

where $N_s = \min[f(\theta_b,\theta_t)]$, and it is known as a stability factor of slope. The N_s-values for various geometries and friction angles may be found in the study by Chen (2).

With N_s known, a least-upper-bound critical height of a slope can be calculated by Equation 14. However, it is observed from the model test results, as shown in Figure 6, that the failure surface of the model slopes did not pass through the toe but passed through a point approximately 20 percent of the height of the slope above the toe. Therefore, to obtain the least-upper-bound critical height of the centrifuged slope, a factor of 1.25 was applied to the solution obtained by Equation 14 to take into account the fact that the failure surface passed approximately 20 percent of the actual height of the slope above the toe. In this manner, the least-upper-bound critical heights of the centrifuged slopes were calculated at three different densities for both soils and are given in Table 3. For these calculations, soil strengths obtained from triaxial testing reported by Kim (3) were used.

Finite-Element Analysis

The finite-element method (FEM) was used to find a lower-bound solution for the given slope problem. The lower-bound theorem of the limit analysis can be stated as follows: If a state of stress can be

Table 3. Results of limit analysis.

Density γ (pcf)	Cohesion c (psi)	N_S	H_c^* (in)	H_c[a]
Soil A				
106.0	0.56	20.26	185.0	231.3
108.0	0.66	23.02	243.1	303.9
110.0	0.76	25.88	309.0	386.3
Soil B				
99.5	0.51	18.48	163.7	204.6
100.5	0.54	19.35	179.7	224.6
101.5	0.57	20.19	195.9	244.9

[a]Equals $1.25 \times H_c^*$.

Figure 8. Mohr circle plot for calculation of factor of safety.

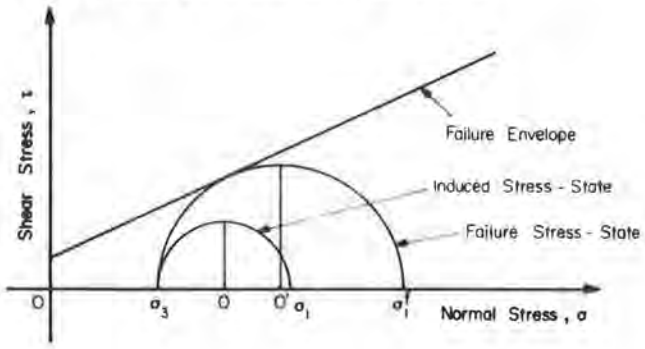

found that satisfies the stress equilibrium and boundary conditions and that does not exceed the yield condition, then no collapse occurs. By the FEM, a state of stress can be found that satisfies the stress equilibrium and boundary conditions. Therefore, if the maximum loading condition is found that induces a state of stress without violating the yield condition anywhere in the structure, it will provide the highest lower-bound solution.

An eight-node isoparametric quadrilateral finite-element program SLOPE was developed for the slope stability analysis during the course of this investigation. In the program SLOPE, nonlinear stress-dependent stress-strain behavior of soil was approximated by a hyperbolic function (4,5), and the incremental tangential Young's modulus E was evaluated by differentiating the function (6). Poisson's ratio was assumed to be 0.35, which is a typical value for partly saturated soils.

In this analysis, failure of an element is assumed to occur when the magnitude of the shear stress developed in an element reaches that of the shear strength. A factor of safety is defined as the ratio of the maximum shear stress induced to the maximum shear stress allowable, which can be visualized on a two-dimensional Mohr circle plot as shown in Figure 8. In Figure 8, the ratio of the radius of the small circle representing the actual stress state induced to the radius of the larger circle representing the stress state at failure represents the factor of safety.

A failure surface is obtained from the factors of safety calculated for assigned elements by finding a continuous line connecting the combination of elements having the smallest overall factor of safety. The continuous line forming a failure surface is assumed to be a circular arc that passes through the top crest of the slope. The overall factor of safety for the entire failure surface F_s can be calculated by the following expression (7):

$$F_s = \sum_{i=1}^{n} (\ell_i/L) f_{si} \qquad (15)$$

Figure 9. Trial failure surfaces of finite-element analysis.

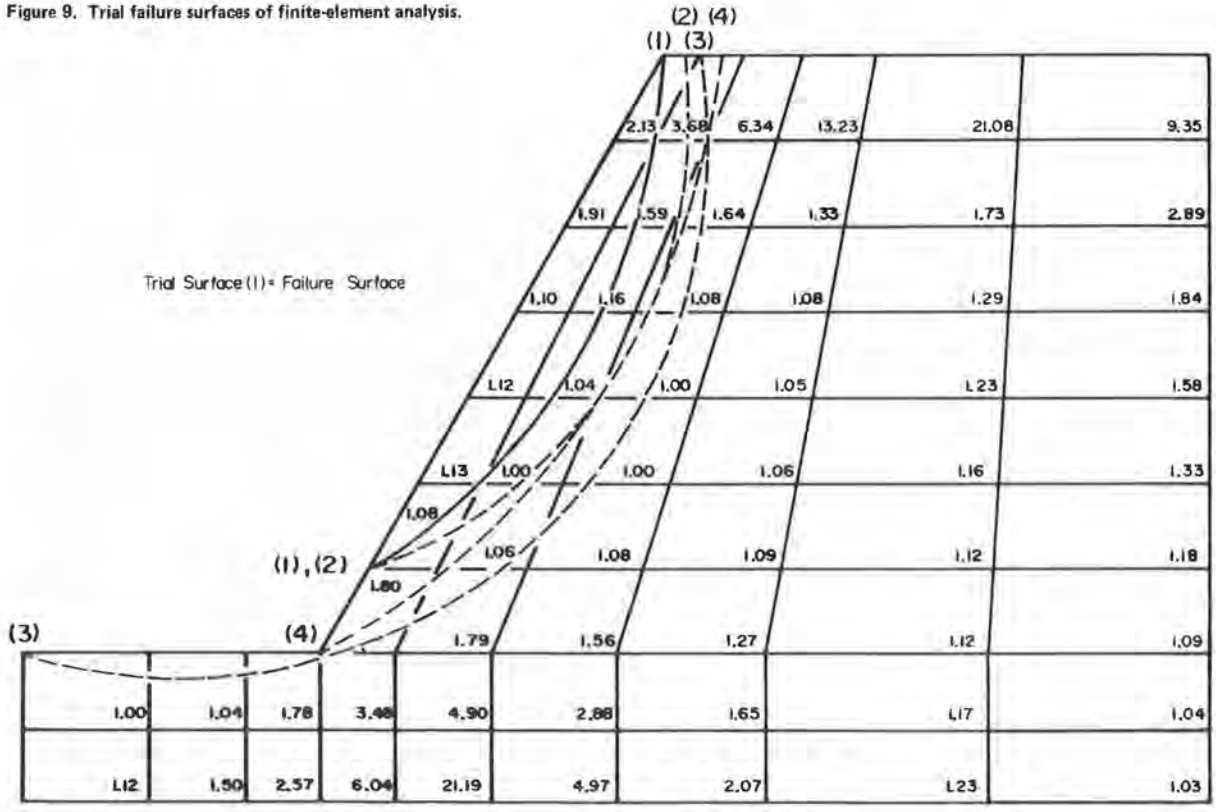

Figure 10. Failure surfaces obtained by SNOB for soils A and B at various densities.

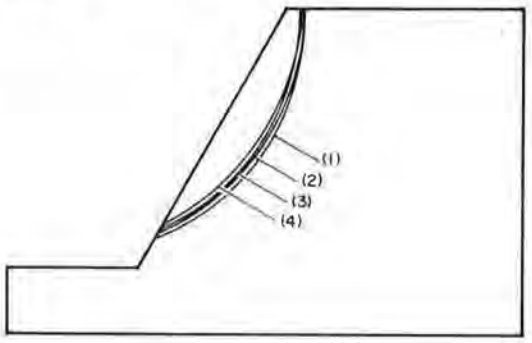

Figure 11. Comparison of results in terms of H_c^p for soil A.

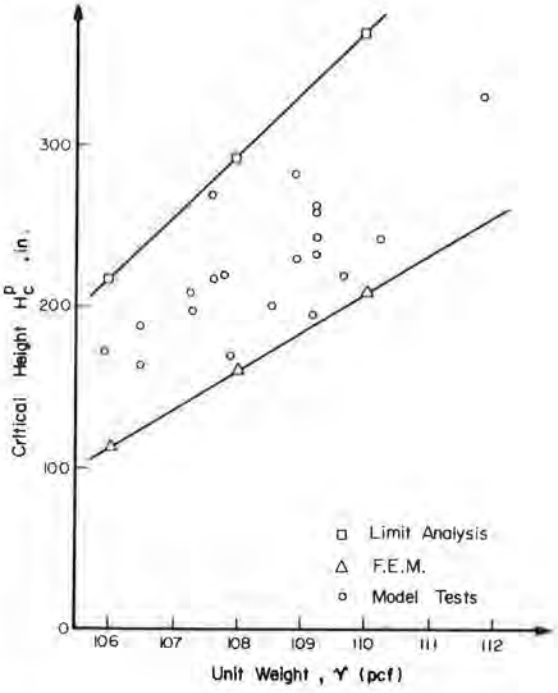

where

f_{si} = factor of safety of element i along failure surface,
ℓ_i = length of failure surface through element i,
L = total length of failure surface, and
n = number of elements on failure surface.

Four trial failure surfaces of circular arcs, which were selected so as to pass through the elements having smaller f_{si}'s than those of the surrounding elements, are shown in Figure 9. Also shown in Figure 9 is the f_{si} of each element at the critical point when any of the elements in the slope first reached an f_{si} equal to or less than unity on increased gravity loading. The overall F_s's of surfaces 1, 2, 3, and 4, calculated by Equation 15, were 1.29, 1.41, 1.50, and 1.57, respectively. Thus, surface 1, which has the smallest failure surface, is chosen to be the failure surface.

Since the procedure of incremental loading by body forces is employed in this method, the critical height of the slope is not directly determined, but the increased unit weight of the soil at the critical point is known, from which the equivalent critical height may be calculated by the following equation:

$$H_c = H_m(\gamma_f/\gamma) \quad (16)$$

where

H_m = height of a numerical model,
γ = initial unit weight of soil in model, and
γ_f = unit weight of soil at critical point.

The critical heights predicted by the FEM at three different densities of the two soils are given below:

Soil	Density γ (pcf)	Critical Height Hc (in)
A	106.0	120
	108.0	168
	110.0	216
B	99.5	104
	100.5	112
	101.5	128

Figure 12. Comparison of results in terms of H_c^p for soil B.

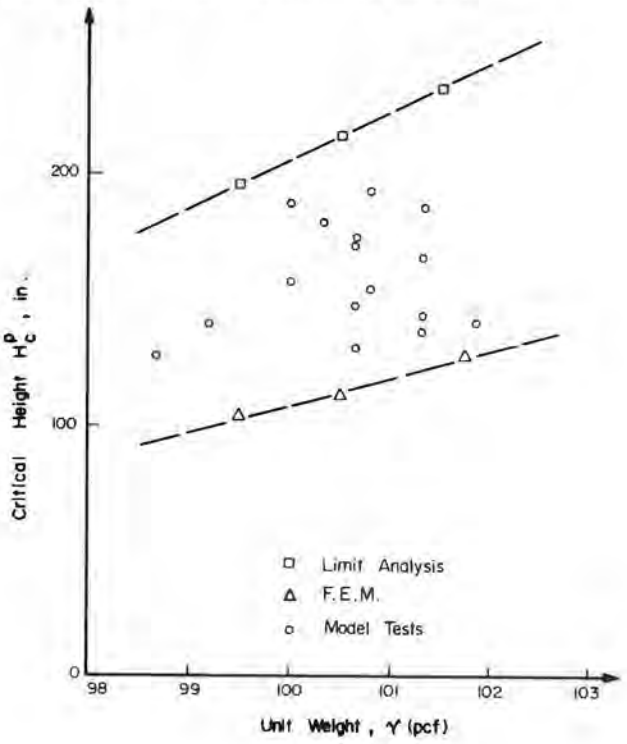

Figure 13. Comparison of failure surfaces.

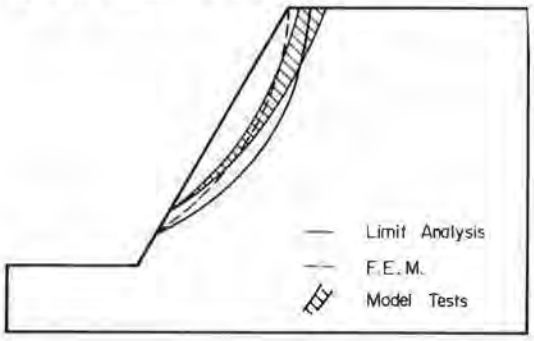

Limiting-Equilibrium Analysis

The limiting-equilibrium slope stability program SNOB (stability--New York and Bishop) (8,9), which uses the simplified Bishop method of the analysis, was used to analyze the slopes for which the heights had previously been determined by limit analysis. Failure surfaces giving the minimum F_s's were obtained by an automatic searching method provided by SNOB and are shown in Figure 10. Soil types and densities for each failure surface are as follows: 1, soil B at 99.5 and 100.5 pcf; 2, soil A at 108.0 pcf; 3, soil A at 106.0 pcf and soil B at 101.5 pcf; and 4, soil A at 110.0 pcf. It is observed that the location of the failure surface is not very sensitive to the small changes of the densities of soil. Therefore, failure surface 2 will represent the failure surfaces when they are compared with those obtained by the FEM and the centrifugal model tests. The average minimum F_s of the slopes predicted by the limit analysis was 0.99. Since the slopes analyzed by the limiting-equilibrium method had the same height as that calculated by the upper-bound method of limit analysis, this implies that the simplified Bishop method used also produces upper-bound solutions. This is not generally the case, since in most limiting-equilibrium analyses, equilibrium (either force or moment) is not satisfied.

MODEL TEST RESULTS VERSUS ANALYTICAL SOLUTIONS

The critical heights of prototype slopes predicted by the upper-bound method of limit analysis and the lower-bound method of finite-element analysis are plotted against the densities of slope soils in Figures 11 and 12 for soils A and B, respectively; the centrifugal model test data are also shown. It is observed from Figures 11 and 12 that all the data points of the centrifugal model tests, in spite of the relatively large scatters, lie between the upper and lower bounds obtained by limit analysis and finite-element analysis, respectively. It is thus concluded from the observation that in slope stability the centrifugal model testing scheme gives consistent results with those of analytical methods such as limit analysis and finite-element analysis in terms of the critical height of a slope.

The failure surfaces obtained by the FEM and computer program SNOB are shown in Figure 13 superimposed on the failure surfaces observed in the centrifugal model tests, which are shown as contained in the band indicated. In general, the failure surface of a slope belongs to one of three different modes depending on whether it passes through the toe, below the toe, or above the toe of the slope. It is observed in Figure 13 that all the failure surfaces shown belong to the same mode passing above the toe, are shallow in depth, and are located sufficiently close to each other to allow us to conclude that the centrifugal model testing scheme also gives consistent results with those of the FEM and the simplified Bishop method in terms of the location of the failure surface.

DISCUSSION AND CONCLUSIONS

In both the centrifugal model tests and the finite-element analysis, the loading was applied as increasing gravity forces on the structure. Although such loading is certainly not the same as that in the case of an actual slope constructed incrementally, it has been shown by finite-element analysis (10) that the two methods of load application do not make much difference in the predicted critical slope height. By the same token, it can thus be argued that centrifugal tests of constructed models would produce similar results as tests in which the model is built up while the centrifuge is in flight. The latter is, of course, a much more difficult experiment to perform.

From the results of the investigation reported in this paper, it can be concluded that centrifugal modeling of slope stability problems gives self-consistent results. Quantitatively, the model test data also agree well with the results from well-established methods of analysis.

Although centrifugal modeling as a tool is becoming familiar to the geotechnical engineer, it should be pointed out that there are several ways in which it could be used. A centrifuge can be used to model a prototype design by constructing a model of it to include all the necessary details. A large centrifuge, of several hundred g-ton capacity, would be required. In the absence of such large facilities, small centrifuges of the size used in this investigation can still be used to test models to gather data for the validation of analytical methods. The analyses can be performed to simulate the test conditions in the centrifuge experiments in which the material properties and loading and boundary conditions are known exactly. In this manner, the feedback from the comparison between test data and analytical results can lead to an improvement in the design methods. Finally, centrifuge experiments can also be conducted for the purpose of observing the phenomena that could take place in the test structure under proper simulation of the gravity stress gradient. When such phenomena are properly understood, numerical models can be formulated to incorporate such effects into analysis and design. The operation of small centrifuges is inexpensive and many experiments can be run for parametric studies. It is foreseen that in the near future such facilities will be available to many geotechnical engineers for the purposes just described.

REFERENCES

1. E. Fumagalli. Statical and Geomechanical Models. Springer-Verlag, Vienna, 1973.
2. W.F. Chen. Limit Analysis and Soil Plasticity. Elsevier Scientific Publishing Co., New York, 1975.
3. M.M. Kim. Centrifuge Model Testing of Soil Slopes. Department of Civil Engineering, Univ. of Colorado, Boulder, Ph.D. thesis, 1980.
4. R.L. Kondner. Hyperbolic Stress-Strain Response: Cohesive Soils. Journal of Division of Soil Mechanics and Foundation Engineering of ASCE, Vol. 89, No. SM 1, Proc. Paper 3429, 1963, pp. 115-143.
5. R.L. Kondner and J.S. Zelasko. A Hyperbolic Stress-Strain Formulation for Sands. Proc., Second Pan American Conference on Soil Mechanics and Foundation Engineering, Brazil, Vol. 1, 1963, pp. 289-324.
6. J.M. Duncan and C.Y. Chang. Non-Linear Analysis of Stress and Strains in Soils. Journal of Division of Soil Mechanics and Foundation Engineering of ASCE, Vol. 96, No. SM 5, 1970, pp. 1629-1653.
7. E.L. Corp, R.L. Schuster, and M.M. McDonald. Elastic-Plastic Stability Analysis of Mine-Waste Embankments. U.S. Bureau of Mines, RI 8069, 1975.
8. S.J. Hasselquist and R.L. Schiffman. A Computer Program for Slope Stability: New York State and Simplified Bishop Method. Computing Center, Univ. of Colorado, Boulder, Rept. 74-5, 1974.
9. R.M. Leary. Computerized Analysis of the Stability of Earth Slopes. Bureau of Soil Mechanics, New York State Department of Transpor-

tation, Albany, Soil Design Procedure SDP-1, 1970.
10. I.M. Smith and R. Hobbs. Finite Element Analysis of Centrifuged and Built-Up Slopes. Geotechnique, Vol. 24, No. 4, 1974, pp. 531-559.

Publication of this paper sponsored by Committee on Mechanics of Earth Masses and Layered Systems.

Rectangular Open-Pit Excavations Modeled in Geotechnical Centrifuge

O. KUSAKABE AND A.N. SCHOFIELD

Tests of models made of soil in geotechnical centrifuges have become accepted as a method of study of mechanisms of ground deformation with less expense or delay and with more control of ground conditions than tests of prototype scale. Centrifuge test results are reported for four different rectangular open pits excavated rapidly in saturated clay soil of uniform strength with depth. It is found that the mechanism by which such excavation will cause road pavements and buried services to fail will fit the axisymmetric mechanism, where the upper part of the pit wall tends only to move vertically and the wall movement is dominated by plastic deformation of the lower part of the pit wall. Support in the upper region will have little effect on this axisymmetric mechanism, and the stability of the pit will be controlled by the strength of the ground near the base of the excavation. The observed mechanism induces tension in the upper portion of the ground and induces compression failure at depth. Flexible road construction is rather weak in tension, so the observed mechanism is probably relevant to pits passing through a flexible road construction and entering a lower layer of soft ground.

The excavation of trenches or of pits in roads can cause damage to road pavements or to buried services beside the excavation. Ground movements at failure can be fitted to failure mechanisms of the theory of plasticity. Studies of ground movements before failure show that the incipient failure mechanism is established well before failure occurs and that damaging ground movements increase rapidly as the factor of safety against failure is reduced. Tests of models made of soil in geotechnical centrifuges have become accepted as a method of study of mechanisms of ground deformation with less expense or delay and with more control of ground conditions than tests of prototype scale. This paper is concerned with the modeling of rectangular open pits excavated rapidly in saturated clay soil of uniform strength with depth.

The failure of a long trench is illustrated in Figure 1a, with a vertical face ABC moving down into the trench as soil slips on an inclined plane CD and a tension crack DE opens. The failure of a circular shaft is illustrated in Figure 1b and 1c. In the rapid undrained failure (Figure 1b), the lower portion BC of the vertical face squeezes in and an annular ring of soil of section BCD is plastically compressed and deformed. Above the plastic zone BCD a rigid block ABDE descends vertically; there is shearing on DE as well as on CD, on DB, and within BCD (1). In the long term, shown in Figure 1c, a shaft that is safe against rapid failure may exhibit a crack at B and subsequently begin to cave in. This paper reports tests of four different model rectangular open-trench or pit excavations; their behavior can be compared with these plane and axisymmetric cases.

The tests used Speswhite kaolin clay soil reconstituted from a slurry. It was consolidated with vertical effective stress σ_v' = 140 kN/m² and allowed to swell back into equilibrium in centrifuge flight with stresses $0 \leq \sigma_v' < 140$ kN/m² as shown in Figure 2. When rapidly sheared, such soil has shear strength $24 < c_u < 32$ kN/m² throughout the model depth. In such rapid shearing the effective mean normal stress in the clay approaches a critical state pressure (in this case, say, p' = 62 kN/m²) and the pore-water pressures take whatever value is needed to balance externally applied total pressure. In the longer term, excess pore-water pressure gradients will lead to the flow of pore water. A point of particular interest in these tests is the observation of pore-water pressure changes in the clay during and after the process of excavation.

CENTRIFUGE MODEL TEST SYSTEM

In centrifuge model tests, the weight of soil is increased and the scale of the model is reduced, both by a factor n (2). The result is identical similarity at corresponding points in a model and in a notional full-scale prototype of the total and effective stresses and strains in the soil and of the pore-water pressures. In addition, the reduction of model scale by a factor of n means that pore-water diffusion to achieve a given time factor ($T_v = C_v t/h^2$ in Terzaghi's consolidation theory) requires times t_m in the model greatly reduced in comparison with times t_p in the prototype in the ratio $t_m/t_p = 1/n^2$. In this paper, tests will be reported with axes on graphs both at the model and at the notional prototype scale. Details of the model excavation dimensions are shown in Figure 3; positions of pore-water pressure transducers (PA, PB, and PC) and of displacement transducers [linear variable differential transformers (LVDTs), LR, LS, and LT] are shown in the plan for each model at model scale.

The models were made in a circular tub of internal diameter 850 mm (designated 1 in Figure 4). The clay (2) was consolidated and the pit (3) excavated and lined with a rubber bag (4) containing a bag pressure transducer (5). The bag was filled with a heavy fluid $ZnCl_2$ solution (3). Pore-water transducers A, B, and C had been consolidated into position 7. Lead powder threads were injected into the clay (8), and lead shot was placed on various surfaces. These would allow study of deformation during dissection of the model. In flight there were LVDT measurements that followed surface movements.